Infrared thermography as a non-invasive scanner for concealed weapon detection

WeeLiam Khor[1,2†], Yichen Kelly Chen[3], Michael Roberts[3,4], Francesco Ciampa[1]

[1] Department of Mechanical Engineering Sciences, University of Surrey, Guildford GU2 7XH, United Kingdom.
[2] Department of Technology, Design and Environment, Oxford Brookes University, Wheatley, OX33 1HX, United Kingdom.
[3] Department of Applied Mathematics and Theoretical Physics, University of Cambridge, Wilberforce Road, Cambridge, CB3 0WA, United Kingdom.
[4] Department of Medicine, University of Cambridge, Hills Road, Cambridge, CB2 2QQ, United Kingdom.

[†]Corresponding author: wkhor@brookes.ac.uk

Abstract

Non-invasive scanning techniques are vital for threat detection in areas of heavy human traffic to ensure civilian safety. Longer waves in the electromagnetic spectrum, such as millimetre waves and terahertz, have been successfully deployed in commercial personnel scanning systems. However, these waves suffer from lower image resolution due to their longer wavelengths.

Infrared has a shorter wavelength compared to millimetre waves and terahertz. Infrared has a lower penetration potential compared to its counterparts but boosts higher image resolution due to its shorter wavelength. Machine learning techniques, i.e., principal component analysis, active contour, and Fuzzy-c, were applied to the infrared images to improve the visualization of concealed objects.

Convolutional neural networks, i.e., ResNet-50, were explored as an automatic classifier for the presence of concealed objects. A transfer learning approach was applied to an ImageNet pre-trained ResNet-50 model. After preprocessing the IR images using Fuzzy-c, two models were trained, using 900 and 3082 images, respectively. Evaluating the models using a confusion matrix and receiver operating characteristic curve, an area-under-curve of 0.869 and 0.922 was obtained. An optimization procedure was used to determine the model threshold, resulting in a prediction error of 19.9% and 14.9%, respectively.

Keywords: Infrared thermography; convolutional neural networks; principal component analysis; active contour; Fuzzy-c; security scanning; weapon detection.

Introduction

Extremists frequently transport concealed weapons and improvised explosive devices (IEDs) to evade security detection while plotting or carrying out potentially harmful actions against civilians or authorities. Concealed weapons can be classified into three categories: those with wide-area effects (such as poisonous gas or improvised explosive devices), those requiring physical contact (including knives and stun guns), and those used at a distance (like guns and rifles) [1]. Because concealed weapons are typically not visually apparent, security personnel have faced challenges in ascertaining their existence without conducting close physical searches on individuals.

In high-security zones, a comprehensive body x-ray scanner is frequently employed to identify objects concealed on an individual. X-ray technology penetrates the subject, providing a detailed cross-sectional view of both the individual and any concealed items. These scanners are configured to operate from a distance, allowing subjects to be isolated and scanned without their knowledge, potentially causing potential perpetrators to either abort their intended attack or bypass the checkpoint altogether [1].

One of the traditional scanning devices is the X-ray detector [2], which emits X-rays with short wavelengths (ranging from 10-7 m to 10-9 m), high frequencies (from 3 × 1016 Hz to 3 × 1019 Hz), and high energy levels (from 124 keV to 145 eV). X-rays are the most penetrating among all electromagnetic scanners, providing comprehensive information about the subject's cross-section. Nevertheless, the use of X-ray scanners is gradually being phased out due to potential health risks associated with ionizing radiation exposure when human subjects are involved [3-7].

Security applications have harnessed the use of safer electromagnetic waves characterized by longer wavelengths, including millimetre-wave, terahertz, and infrared [1]. Millimetre-wave (MMW) technology has found successful application in devices designed for concealed weapons detection [8]. The technology has been under active research since the 1950s, initially in the form of radiometers [9]. Millimetre-wave (MMW) technology operates within the frequency range of 30–300 GHz, with a wavelength ranging from 1 to 10 mm. It is capable of penetrating conditions with low visibility, such as fog, to bounce signals off the subject [10-12]. However, MMW is generally characterized as narrowband and less effective over longer distances (less than 10 meters), often necessitating proximity between the subject and the sensor [13].

Terahertz (THz), in contrast, is an electromagnetic wave situated between the millimetre-wave (MMW) and infrared (IR) spectra. THz boasts a frequency range from 100 GHz to 10 THz and a wavelength spanning 3 mm to 30 μm. Both MMW and THz exhibit effective penetration capabilities through standard clothing [14]. The achievements of THz technology in security scanning applications have culminated in the creation of a commercial personnel scanning system by Thruvision [15, 16].

Passive IR thermography in security scanning measures the natural IR signature emitted by human bodies using an IR camera, without having to expose the subject to any amount of radiation [17]. It also does not acquire human interpretable facial features during detection, thus IR scanners safeguard both the subject’s health and privacy [17]. Another additional advantage is that a passive IR system does not project waves to illuminate the target subject [18], avoiding potential detection using another IR system.

Passive infrared (IR) thermography has been employed to identify concealed objects on individuals, yielding varying degrees of success. In this approach, the human subject serves as the thermal heat source, emitting heat that interacts with concealed objects before dissipating through the outermost clothing layer. Consequently, areas on the outer clothing layer, where concealed objects are located, emit infrared radiation at differing rates, potentially manifesting these objects in thermographic images.

One notable advantage of using IR cameras is their relative cost-effectiveness in comparison to MMW and THz systems. Furthermore, IR systems operate with shorter wavelengths than MMW and THz devices, enabling the potential for higher-resolution images, which permits IR systems to be situated at greater distances for image capture [19, 20]. Additionally, IR cameras facilitate high-volume applications, as they are capable of simultaneously visualizing numerous individuals and objects in large areas. Modern IR cameras typically offer high resolutions, such as 640 × 512 pixels, with a typical field of view (FOV) spanning 22 degrees horizontally and 16 degrees vertically [19, 20].

Nonetheless, research has demonstrated that signal penetration through clothing increases with wavelength [21], resulting in reduced signals when scanning through thicker clothing layers [22-24]. Consequently, many attempts to employ electromagnetic waves for concealed object detection have gravitated toward MMW or THz technologies due to their superior wave penetration capabilities [14]. Despite IR's comparatively limited penetration, resulting in reduced signals reflected from clothing surfaces, machine learning (ML) techniques can be harnessed to process IR data, enhancing the effectiveness of the detection system. ML methods applied to IR data have previously shown success in addressing challenges such as damage detection in composites and object segmentation [25-30].

An ideal system should be both portable and capable of standoff and walk-through detection of concealed IEDs and weapons, regardless of their size or the layers of clothing covering them. This system should possess a wide field of view (FOV) to cover extended distances and deliver precise results in large areas, ultimately enabling a faster throughput and a more cost-effective screening process. The integration of IR imaging technology with ML data processing algorithms holds the potential to encompass all of these essential features.

This paper addresses, the potential of a ML-based thermal imaging system as a standalone IR detector for objects concealed underneath clothing. The paper outlines two objectives: improving the visualisation of a concealed object, and automatic detection of concealed objects using convolutional neural networks (CNN). Machine learning techniques, such as principal component analysis, Chan-Vese active contour and Fuzzy-c respectively, for image segmentation and data reduction, thus enabling the visualisation of the target object. ResNet-50 was opted as the CNN for classification.

Methodology

Data acquisition

In our experiments, our goal is to replicate a checkpoint detection scenario where a subject walks through a predetermined narrow passage at a specific distance from the IR detector. We employed a square neoprene rubber target to simulate a concealed IED and utilized layered windproof clothing as the outer clothing (Figure 1). A thin layered clothing is worn beneath the concealed object. An image of the subject with exposed object is shown in Figure 1 (c).

(a)

(b)

(c)

Figure 1 The concealed object and layered windproof used in the experiments are shown in (a) and (b). The target subject wearing a layered windproof with exposed object is shown in (c).

The FLIR A6750sc Mid Wavelength IR camera was used to capture thermal data. The camera captures IR images in 640 × 512 pixels in resolution, operates in the range of 3 - 5 µm waveband with a thermal sensitivity of < 20 mK. The IR camera was left on a fixed and stable location for data capture. The subject was positioned approximately 3 meters away from the camera to enable better resolution in the upper torso area (Figure 2). The ambient temperature during data collection was measured to be at 22.0 °C. The camera lens was adjusted to focus on the subject's position and fixed prior to data capture. For the analysis, one image was captured with the static background, and another was taken with the subject in position.

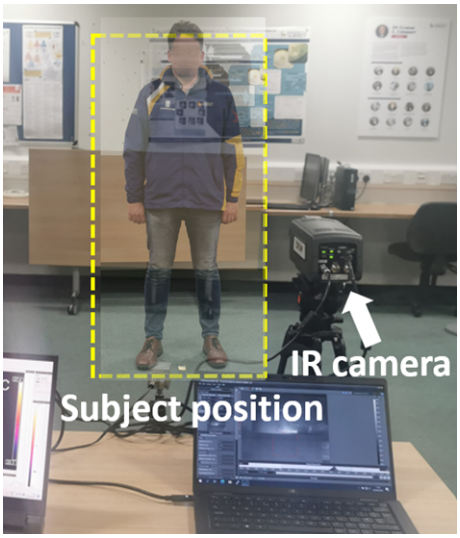

Figure 2 IR camera setup for data collection.

Background removal by Principal Component Analysis

For this first stage, PCA was used to remove background information, whilst retaining information on the subject and object [25]. PCA is a linear dimensionality reduction technique that transforms a set of correlated variables (p) into a smaller number (k, where $k < p$) of uncorrelated variables, called principal components (PCs) [23, 24]. Each PC is a linear combination of original variables, and the magnitude of coefficients in this linear combination represents the contribution of each original variable to a specific PC. PCs are ordered such that the first PC explains the most variance, and each subsequent PC explains as much of the remaining unexplained variance as possible. A comprehensive mathematical framework of PCA applied to thermal data is found for example in reference [18]. For background removal, both the background scene and the image with the subject (with or without the object) were processed by PCA. Pixels with large correlated intensity variation between images would have large coefficients (by magnitude) for the first PC. In the current work, these pixels corresponded to the region occupied by the subject.

Subject segmentation by Active Contour

Following PCA, active contour techniques were applied to segment the subject from the background, resulting in a clean, noiseless background. The Chan-Vese active contour method was employed, where an iterative algorithm updates the shape and position of one or more contours, aiming to ensure that pixels inside the contours are as homogeneous to each other as possible, and similarly, pixels outside the contours are as homogeneous to each other as possible, but different from those inside [31, 32].

Information reduction by Fuzzy-c clustering

The Fuzzy-c method was used as the unsupervised ML technique for clustering of thermal data and image segmentation [25]. The Fuzzy-c clustering method require initial cluster centres to initiate cluster association, followed by the calculation of distance-based membership scores to indicate how strongly each pixel associates to each cluster. Scores are then used to update cluster centres by putting more emphasis on pixels that have stronger association. This process is repeated until a stopping criterion is reached.

ResNet-50 Convolutional Neural Network for classification

ResNet-50[33] was used as the CNN model used to classify the IR images. CNNs are a class of versatile deep learning network architecture, commonly used for image classification. For image classification, the input image undergoes a series of convolutional, pooling, fully-connected, and classification layers, which produces an output of probability values for different classes.

Usually, when training a CNN model from the ground up, the prevailing recommendation is to ensure that the training dataset is at least an order of magnitude larger than the test dataset. This approach enhances diversity and helps prevent overfitting [34, 35]. Nonetheless, properly annotated infrared datasets for individuals with concealed objects are scarce and are frequently not made available to the public. To address the challenge of limited dataset size, we employed a pre-trained ResNet-50 model. The model was pre-trained using the ImageNet dataset [36], which contained 1.4 million natural images with 1000 classes.

The transfer learning approach was taken to further train the pre-trained model fit our task. Fuzzy-c was used to preprocess both training and test dataset due to improved performance compared to raw images. To develop the models, the fully connected layer was fine-tuned using a smaller and a larger dataset respectively, corresponding to 900 (462 with and 438 without object) and 3082 (1918 with and 1164 without object) labelled images. The fundamental principle of the transfer learning approach is that the generic features extracted from an extensive dataset (i.e. ImageNet) are transferable and informative across diverse datasets. This versatility of learned generic features is a distinctive advantage of deep learning, enabling their application in a range of domain-specific tasks even when working with limited

datasets [37]. Using MATLAB's Deep Network Designer, the fully connected layer in the pre-trained model was modified to train using a weight learn rate factor and bias learn rate factor of 10.

For training of the model, transformations were performed by applying rotation by ±45°, reflection on the Y-axis, and rescaling by ±25%. Internal validation was performed using 30% of randomly sampled training data to monitor the training process. Stochastic gradient descent , SGD was used as the optimizer with an initial learning rate of 0.0001, validation frequency of 5, maximum epoch of 20 and a mini batch size of 10. Validation accuracies 95.19% and 96.76% were obtained for the small and large dataset models respectively.

To test the model for performance, a dataset independent to both training datasets consisting 850 images was used (678 with and 172 without object). For the purpose of building a Receiver-Operator Characteristic curve, ROC curve (elaborated below), 344 images (172 with and 172 without object) were randomly picked from this dataset.

		Actual class	
		Positive	**Negative**
Predicted class	**Positive**	*TP*	*FP*
	Negative	*FN*	*TN*

Figure 3 Confusion matrix for model evaluation.

For model evaluation, a ROC curve was used. The ROC curve is a 2D diagram that is built using the True Positive Rate (TPR) and False Positive Rate (FPR) calculated using metrics from the confusion matrix (Figure 3) while applying a tentative cut-off using the predicted probabilities. TPR and FPR are given by,

$$TPR = \frac{\Sigma TP}{\Sigma(TP+FN)}, \tag{5a}$$

$$FPR = \frac{\Sigma FP}{\Sigma(FP+TN)}. \tag{5b}$$

The TPR and FPR are metrics to evaluate the correct predictions of the model. Integrating the ROC curve, an area-under curve, AUC can be obtained. The ROC curve was built 10 times for each model, where 10 corresponding AUC was obtained. The AUC from the same model was averaged to obtain a representative AUC. The AUC is a performance metric for the models, where 0.5 suggests no discrimination, 0.7 to 0.8 is considered acceptable, 0.8 to 0.9 is considered excellent, and > 0.9 is outstanding [38].

Results and discussion

Object visualisation

An example of the background image obtained from the IR camera is shown in Figure 4. Temperature ranging from 20.6°C and 24.3°C were seen in the figure, corresponding to the artifacts in the background.

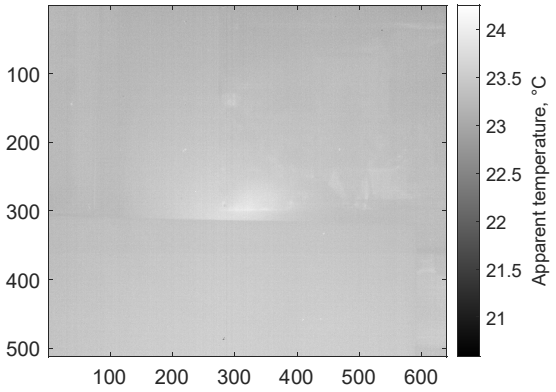

Figure 4 Raw data from IR camera, showing the static background without subject.

An image of the subject with a concealed object under the windproof is shown in Figure 5 (a). The apparent temperature measures between 20.7°C and 34.4 °C, whilst the exposed skin showed temperatures above 30.0°C. Around the surface of the clothing on concealed object area, slightly lower temperature was observed compared to the overall clothing, consistent with observations from other researchers [39-42].

PCA was applied by processing both the background and subject images (Figure 4 and Figure 5 (a) respectively), followed by reforming the image using the first principal component (Figure 5 (b)). The first principal component shows the variation in the pixels between the background and target image. The application of Chan-Vese active contour segmentation on the first principal component reformed image segments the subject from the background. The pixels retained after active contour segmentation were used as markers for information to retain from the raw image. A subject cropped image with 'clean' background was produced by extracting information from the raw image in Figure 5(a) using the segmented markers (Figure 5(c)).

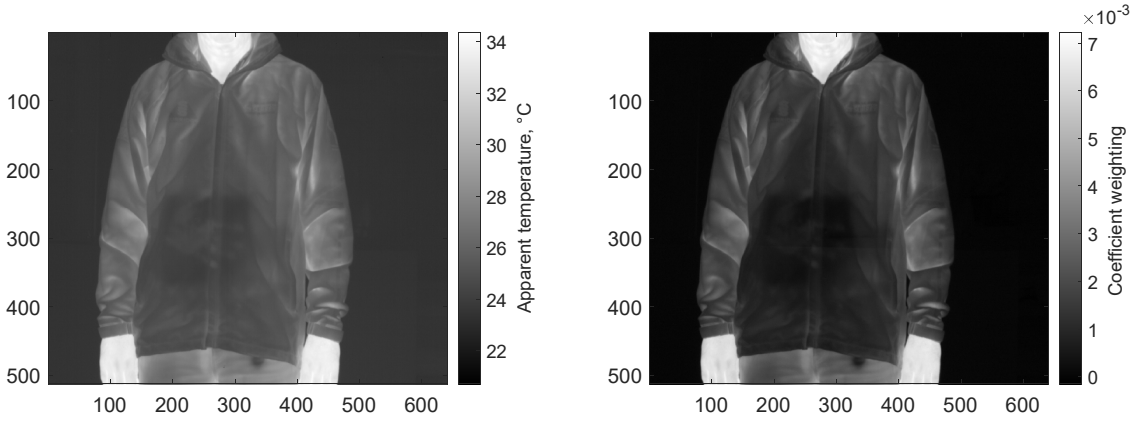

(a) (b)

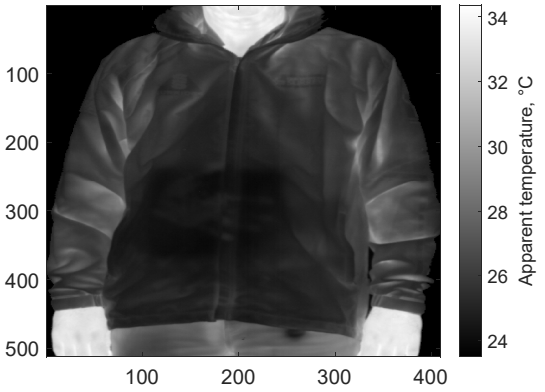

(c)

Figure 5 An illustration of (a) raw data from IR camera, showing subject with concealed object, (b) first principal component, (c) ROI cropped and segmented subject by using the Chan-Vese active contour on PC1.

Although the concealed object area in Figure 5(c) is faintly visible, it would be challenging for a human operator to recognise this in a real detection scenario, where hundreds or more subjects were assessed in a consecutive manner. To tackle such challenges, a data reduction technique, Fuzzy-c was used to further process the ROI segmented image. In this practice, the image illustration of 256 bins was reduced to 16 bins using Fuzzy-c, shown in Figure 6(a).

The Fuzzy-c algorithm clusters the surface of the skin and background into clusters 16 and 1 respectively. Considering that the concealed object area is generally lower than the body and average surface of the clothing, cluster 2 was used as marker to represent the object area (Figure 6(b)). A shape loosely resembling the concealed object Figure 1(a) was seen in Figure 6(b).

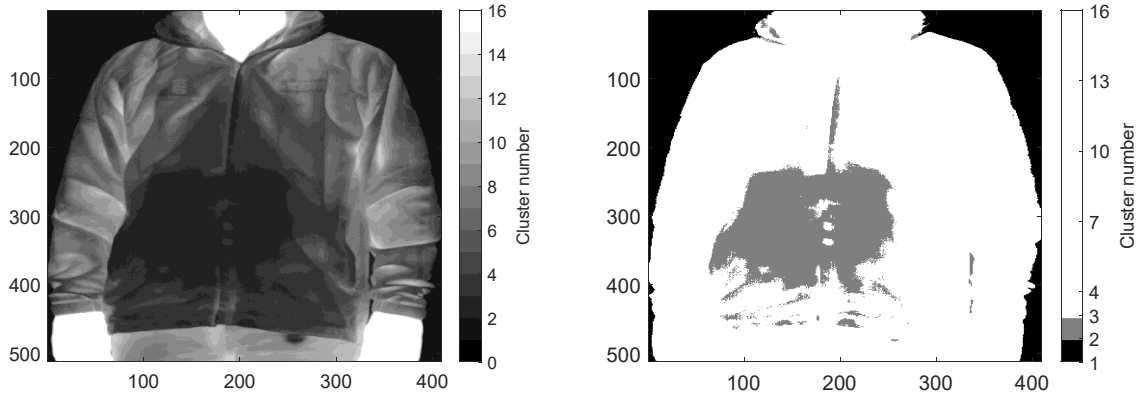

(a) (b)

Figure 6 Processed images of subject with concealed object., showing (a) Fuzzy-c clustering, and (b) Fuzzy-c with emphasis of object area.

Classification using ResNet-50

For image classification, all training and validation images were first processed using Fuzzy-c and ROI sectioning. This is based on preliminary evaluation which found that the postprocessed image model performed better than raw image model.

Two trained ResNet-50 models were compared: smaller dataset model (900 images) and the larger dataset model (3082 images). The larger dataset model contain all images found from the smaller dataset model. ROC curves were built 10 times by randomly selecting 172 images with and without object from the validation dataset for both models. An average AUC of 0.869 and 0.922 was obtained for the smaller and larger dataset Fuzzy-c models respectively (Figure 7).

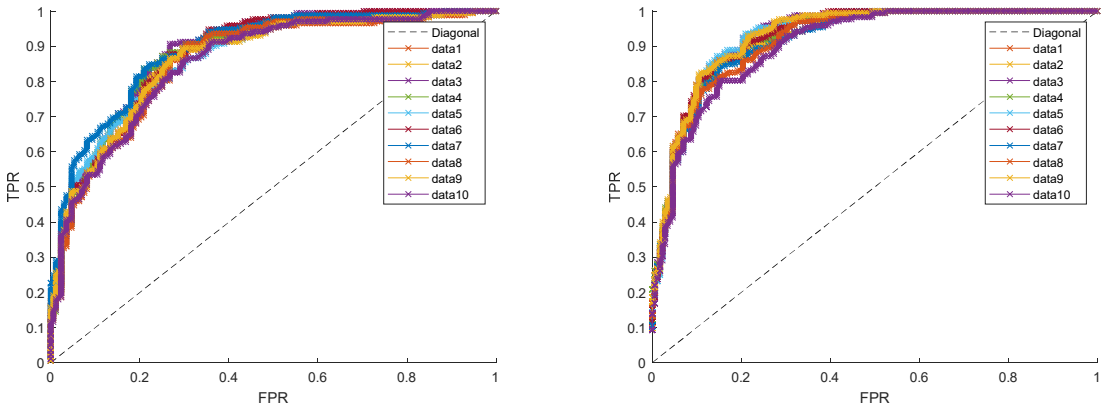

(a) (b)

Figure 7 A compilation of 10 ROC curves each for the (a) smaller and (b) larger dataset Fuzzy-c models.

The image label and corresponding model prediction for the validation set were plotted in Figure 8. In the smaller dataset model, there were more wrongly predicted labels in the top left (false negative) and bottom middle (false positive) of the figure compared to the larger dataset model.

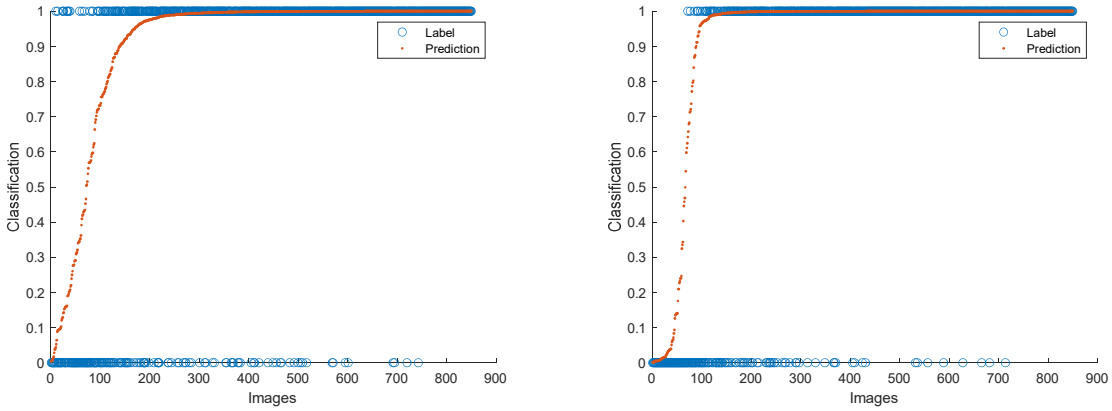

(a) (b)

Figure 8 Label and the corresponding prediction from the (a) smaller and (b) larger dataset Fuzzy-c model.

To determine a cut-off threshold for the model to use in making classification decisions, it is necessary to maximize true positives and negatives while minimizing false positives and negatives. The cut-off threshold can be optimized by identifying the maximum value in the threshold vs. (TPR – FPR) plot (Figure 9). In the case of the small dataset model, the maximum (TPR – FPR) value of 0.6029 corresponds to a threshold of 0.9825, while for the larger dataset model, the maximum (TPR – FPR) value of 0.7017 corresponds to a threshold of 0.9992. These thresholds will then be applied to the model's predictions on the validation dataset to quantify model prediction error.

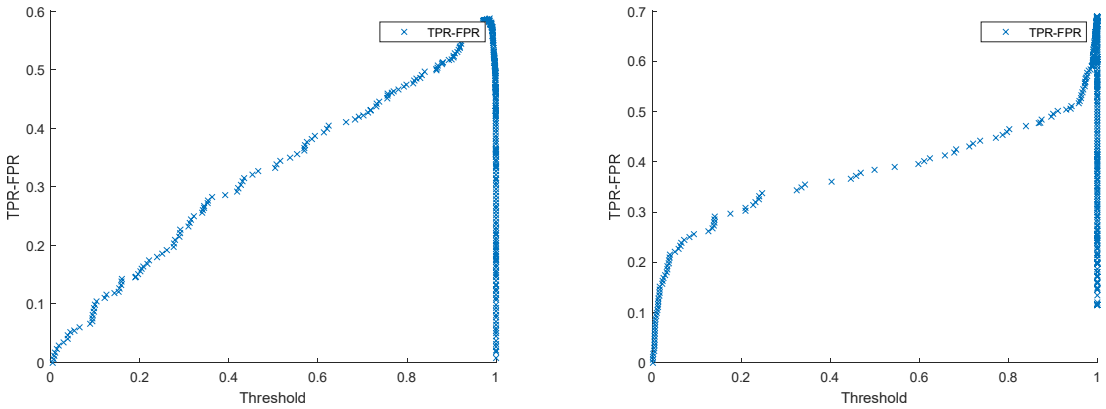

(a) (b)

Figure 9 The threshold vs. (TPR – FPR) plot for the (a) smaller and (b) larger dataset Fuzzy-c models.

A normalised quantification of label is shown in the form of confusion matrix (Figure 10). Overall, both models performed generally well, while the larger dataset model performed better with an overall 14.9% error, compared to the 19.9% error in the smaller dataset model. In general, the larger dataset model performed better than the smaller dataset model in almost all metrics. The difference in dataset size showed that the increase in training dataset can certainly be helpful in improving model accuracy. However, it also highlight the effectiveness of transfer learning for model training, where a model trained with 900 images (smaller dataset model) managed to perform well with an average AUC of 0.869 on a validation dataset of 850 images.

	Label True	Label False
Pred True	0.4358	0.1343
Pred False	0.0642	0.3657

(a)

	Label True	Label False
Pred True	0.4256	0.0747
Pred False	0.0744	0.4253

(b)

Figure 10 Confusion matrix of the normalised labels for the (a) smaller and (b) larger dataset Fuzzy-c models.

Conclusion

The paper explores the potential of infrared thermography for the detection of concealed objects on human subjects by improving object visualization and using convolutional neural networks, such as ResNet-50, for automatic object presence classification. In comparison to unprocessed infrared images, additional image processing revealed indications of objects beneath clothing. Machine learning techniques, including principal component analysis and Chan-Vese active contour techniques, successfully removed background information, isolating the subject within the image. Data reduction techniques, such as K-means and Fuzzy-c, improved object area visualization compared to raw data, with the latter showing better performance.

Two ResNet-50 convolutional neural network models were trained using datasets containing 900 and 3082 images, respectively. The convolutional neural network approach proved to be effective in classifying object presence, with the 900-image model achieving an average area-under-the-curve (AUC) of 0.869 and the 3082-image model achieving an AUC of 0.922. To further improve classification performance, model training with larger dataset is necessary. However, this underscores the effectiveness of the transfer learning approach for training CNN models in small or limited dataset problems.

Acknowledgements

The authors acknowledge funds provided by the Defence and Security Accelerator (DASA) [grant number ACC2022360] for the IR SCREEN project. Help and support provided by Ian Jupp from DSTL and Colin Cameron from QinetiQ was much appreciated.

Biography

WeeLiam Khor

WeeLiam is currently an Associate Lecturer at Oxford Brookes University. Prior to this, he served as a postdoctoral researcher at the University of Surrey from 2019 to 2023. His research background encompasses a diverse range of areas, including mechanical characterization of materials, fracture mechanics, integrity assessment, image processing, and machine learning.

Yichen Kelly Chen

Yichen is currently a PhD candidate in the University of Cambridge. She was managing a data science team in a bio-pharma company prior to PhD. She is experienced in data science and machine learning techniques for biomedical applications.

Michael Roberts

Michael is a Principal Research Associate in the University of Cambridge. He is a member of the Cambridge Image Analysis group (CIA), leads the BloodCounts! consortium (https://www.bloodcounts.org/) and also leads the algorithm development team for the global COVID-19 AIX-COVNET collaboration (https://covid19ai.maths.cam.ac.uk/).

Francesco Ciampa

Francesco is currently an Associate Professor (Reader) in the University of Surrey. He was ranked among the top 2% of scientists in 2022. He has multi-disciplinary experience in NDE, SHM, numerical and experimental testing of materials and structures for the aerospace and energy sectors.

Reference

[1] National Research Council, "Existing and Potential Standoff Explosives Detection Techniques," (in English), p. 148, 2004, doi: 10.17226/10998.

[2] S. Akçay, M. E. Kundegorski, M. Devereux, and T. P. Breckon, "Transfer learning using convolutional neural networks for object classification within X-ray baggage security imagery," in *2016 IEEE International Conference on Image Processing (ICIP)*, 25-28 Sept. 2016 2016, pp. 1057-1061, doi: 10.1109/ICIP.2016.7532519.

[3] H. D. Barth, M. E. Launey, A. A. MacDowell, J. W. Ager, and R. O. Ritchie, "On the effect of X-ray irradiation on the deformation and fracture behavior of human cortical bone," *Bone,* vol. 46, no. 6, pp. 1475-1485, 2010/06/01/ 2010, doi: https://doi.org/10.1016/j.bone.2010.02.025.

[4] H. D. Barth, E. A. Zimmermann, E. Schaible, S. Y. Tang, T. Alliston, and R. O. Ritchie, "Characterization of the effects of x-ray irradiation on the hierarchical structure and mechanical properties of human cortical bone," *Biomaterials,* vol. 32, no. 34, pp. 8892-8904, 2011/12/01/ 2011, doi: https://doi.org/10.1016/j.biomaterials.2011.08.013.

[5] R. L. Brent, "The effect of embryonic and fetal exposure to x-ray, microwaves, and ultrasound: counseling the pregnant and nonpregnant patient about these risks," (in eng), *Semin Oncol,* vol. 16, no. 5, pp. 347-368, 1989/10// 1989. [Online]. Available: http://europepmc.org/abstract/MED/2678486.

[6] K. Faraj and S. Mohammed, "Effects of chronic exposure of X-ray on hematological parameters in human blood," *Comparative Clinical Pathology,* vol. 27, no. 1, pp. 31-36, 2018/01/01 2018, doi: 10.1007/s00580-017-2547-7.

[7] X. Liang, J. Y. Zhang, I. K. Cheng, and J. Y. Li, "Effect of high energy X-ray irradiation on the nano-mechanical properties of human enamel and dentine," *Brazilliam Oral Research,* vol. 30, no. 9, 2016 doi: https://doi.org/10.1590/1807-3107BOR-2016.vol30.0009.

[8] QinetiQ, "Security screening visitors at a large London venue," 2018. [Online]. Available: https://www.qinetiq.com/-/media/a379b9fbfdc94e03b85988893694a8e6.ashx.

[9] R. Appleby, *The history of passive millimetre-wave imaging at QinetiQ* (SPIE Security + Defence). SPIE, 2008.

[10] C. D. Haworth, Y. De Saint-Pern, D. Clark, E. Trucco, and Y. R. Petillot, "Detection and Tracking of Multiple Metallic Objects in Millimetre-Wave Images," *International Journal of Computer Vision,* vol. 71, no. 2, pp. 183-196, 2007/02/01 2007, doi: 10.1007/s11263-006-6275-8.

[11] C. D. Haworth, Y. De Saint-Pern, Y. R. Petillot, and E. Trucco, "Public security screening for metallic objects with millimetre-wave images," *IET Conference Proceedings,* pp. 1-4. [Online]. Available: https://digital-library.theiet.org/content/conferences/10.1049/ic_20050060

[12] C. Haworth *et al.*, *Image analysis for object detection in millimetre-wave images* (European Symposium on Optics and Photonics for Defence and Security). SPIE, 2004.

[13] A. A. David, D. R. Nacer, E. S. Sarah, B. Nicholas, S. Matthew, and G. B. John, "Detection of concealed explosives at stand-off distances using wide band swept millimetre waves," in *Proc.SPIE*, 2008, vol. 7117, p. 71170J, doi: 10.1117/12.800382. [Online]. Available: https://doi.org/10.1117/12.800382

[14] *Innovations in Defence Support Systems - 2 - Socio-Technical Systems*, 1 ed. (Studies in Computational Intelligence). Berlin, Heidelberg: Springer Berlin, Heidelberg, 2011, pp. XIII, 286.

[15] M. A. Butavicius, K. M. Parsons, A. McCormac, R. Foster, A. Whittenbury, and V. MacLeod, "Assessment of the ThruVision T4000 Passive Terahertz Camera: A Human Factors Case Study," in *Innovations in Defence Support Systems -2: Socio-Technical Systems*, L. C. Jain, E. V. Aidman, and C. Abeynayake Eds. Berlin, Heidelberg: Springer Berlin Heidelberg, 2011, pp. 183-206.

[16] Thruvision, "Profit Protection Product Range." [Online]. Available: https://thruvision.com/download/24953/.

[17] M. Kowalski, A. Grudzień, N. Palka, and M. Szustakowski, *Face recognition in the thermal infrared domain* (SPIE Security + Defence). SPIE, 2017.

[18] R. D. Erik *et al.*, "Active and passive infrared spectroscopy for the detection of environmental threats," in *Proc.SPIE*, 2014, vol. 9106, p. 91060A, doi: 10.1117/12.2058544. [Online]. Available: https://doi.org/10.1117/12.2058544

[19] N. Kukutsu and Y. Kado, "Overview of Millimeter and Terahertz Wave Application Research," *NTT Technical Review,* vol. 7, no. 3, 2009. [Online]. Available: https://www.ntt-review.jp/archive/ntttechnical.php?contents=ntr200903sf1.html#top.

[20] J. Binstock and M. Minukas, "Developing an Operational and Tactical Methodology for Incorporating Existing Technologies to Produce the Highest Probability of Detecting an Individual Wearing an IED," Masters, Naval Postgraduate School, Monterey, California, 2010. [Online]. Available: https://www.hsdl.org/c/view?docid=461606

[21] M. Kowalski, "Real-time concealed object detection and recognition in passive imaging at 250GHz," *Appl. Opt.,* vol. 58, no. 12, pp. 3134-3140, 2019/04/20 2019, doi: 10.1364/AO.58.003134.

[22] M. Slamani, P. K. Varshney, R. M. Rao, M. G. Alford, and D. Ferris, "Image processing tools for the enhancement of concealed weapon detection," in *Proceedings 1999 International Conference on Image Processing (Cat. 99CH36348)*, 24-28 Oct. 1999 1999, vol. 3, pp. 518-522 vol.3, doi: 10.1109/ICIP.1999.817168.

[23] Z. Xue, R. S. Blum, and Y. Li, "Fusion of visual and IR images for concealed weapon detection," in *Proceedings of the Fifth International Conference on Information Fusion. FUSION 2002. (IEEE*

Cat.No.02EX5997), 8-11 July 2002 2002, vol. 2, pp. 1198-1205 vol.2, doi: 10.1109/ICIF.2002.1020949.

[24] M. R. Dickson, "Handheld Infrared camera use for suicide bomb detection: feasibility of use for thermal model comparison," Master of Science, Department of Mechanical and Nuclear Engineering, Kansas State University, Manhattan, Kansas, 2008. [Online]. Available: https://krex.k-state.edu/handle/2097/1045

[25] Z. Wang, L. Wan, N. Xiong, J. Zhu, and F. Ciampa, "Variational level set and fuzzy clustering for enhanced thermal image segmentation and damage assessment," *NDT & E International,* vol. 118, p. 102396, 2021/03/01/ 2021, doi: 10.1016/j.ndteint.2020.102396.

[26] Z. Wang, J. Zhu, G. Tian, and F. Ciampa, "Comparative analysis of eddy current pulsed thermography and long pulse thermography for damage detection in metals and composites," *NDT & E International,* vol. 107, p. 102155, 2019/10/01/ 2019, doi: 10.1016/j.ndteint.2019.102155.

[27] D. Wang, Z. Wang, J. Zhu, and F. Ciampa, "Enhanced pre-processing of thermal data in long pulse thermography using the Levenberg-Marquardt algorithm," *Infrared Physics & Technology,* vol. 99, pp. 158-166, 2019/06/01/ 2019, doi: 10.1016/j.infrared.2019.04.009.

[28] Z. Wang, G. Tian, M. Meo, and F. Ciampa, "Image processing based quantitative damage evaluation in composites with long pulse thermography," *NDT & E International,* vol. 99, pp. 93-104, 2018/10/01/ 2018, doi: 10.1016/j.ndteint.2018.07.004.

[29] B. Chen, W. Wang, and Q. Qin, "Robust multi-stage approach for the detection of moving target from infrared imagery," *Optical Engineering,* vol. 51, no. 6, p. 067006, 2012. [Online]. Available: https://doi.org/10.1117/1.OE.51.6.067006.

[30] P. Cotič, Z. Jagličić, E. Niederleithinger, M. Stoppel, and V. Bosiljkov, "Image Fusion for Improved Detection of Near-Surface Defects in NDT-CE Using Unsupervised Clustering Methods," *Journal of Nondestructive Evaluation,* vol. 33, no. 3, pp. 384-397, 2014/09/01 2014, doi: 10.1007/s10921-014-0232-1.

[31] T. F. Chan and L. A. Vese, "Active contours without edges," *IEEE Transactions on Image Processing,* vol. 10, no. 2, pp. 266-277, 2001, doi: 10.1109/83.902291.

[32] V. Caselles, R. Kimmel, and G. Sapiro, "Geodesic Active Contours," *International Journal of Computer Vision,* vol. 22, no. 1, pp. 61-79, 1997/02/01 1997, doi: 10.1023/A:1007979827043.

[33] K. He, X. Zhang, S. Ren, and J. Sun, "Deep Residual Learning for Image Recognition," in *2016 IEEE Conference on Computer Vision and Pattern Recognition (CVPR)*, 27-30 June 2016 2016, pp. 770-778, doi: 10.1109/CVPR.2016.90.

[34] J. T. Barry-Straume, Adam; Engels, Daniel W.; Fine, Edward, "An Evaluation of Training Size Impact on Validation Accuracy for Optimized Convolutional Neural Networks," *SMU Data Science Review,* vol. 1, 2018. [Online]. Available: https://scholar.smu.edu/datasciencereview/vol1/iss4/12.

[35] K. L. Junghwan Cho, Ellie Shin, Garry Choy, Synho Do, "How much data is needed to train a medical image deep learning system to achieve necessary high accuracy?," *ICLR 2016,* 2016 doi: https://doi.org/10.48550/arXiv.1511.06348.

[36] J. Deng, W. Dong, R. Socher, L. J. Li, L. Kai, and F.-F. Li, "ImageNet: A large-scale hierarchical image database," in *2009 IEEE Conference on Computer Vision and Pattern Recognition*, 20-25 June 2009 2009, pp. 248-255, doi: 10.1109/CVPR.2009.5206848.

[37] R. Yamashita, M. Nishio, R. K. G. Do, and K. Togashi, "Convolutional neural networks: an overview and application in radiology," *Insights into Imaging,* vol. 9, no. 4, pp. 611-629, 2018/08/01 2018, doi: 10.1007/s13244-018-0639-9.

[38] J. N. Mandrekar, "Receiver Operating Characteristic Curve in Diagnostic Test Assessment," *Journal of Thoracic Oncology,* vol. 5, no. 9, pp. 1315-1316, 2010/09/01/ 2010, doi: https://doi.org/10.1097/JTO.0b013e3181ec173d.

[39] M. Kastek, M. Kowalski, H. Polakowski, P. Lagueux, and M.-A. Gagnon, *Passive signatures concealed objects recorded by multispectral and hyperspectral systems in visible, infrared and terahertz range* (SPIE Defense + Security). SPIE, 2014.

[40] M. Kowalski, M. Kastek, N. Palka, H. Polakowski, M. Szustakowski, and M. Piszczek, "Investigations of concealed objects detection in visible, infrared and terahertz ranges," *Photonics Letters of Poland,* vol. 5, pp. 167-169, 12/31 2013, doi: 10.4302/plp.2013.4.16.

[41] M. Kowalski, M. Kastek, and M. Szustakowski, "Concealed Objects Detection in Visible, Infrared and Terahertz Ranges," *International Journal of Computer, Information, Systems and Control Engineering,* vol. 8, pp. 1632-1627, 12/12 2014.

[42] M. Kowalski, M. Kastek, M. Piszczek, M. Życzkowski, and M. Szustakowski, *Harmless screening of humans for the detection of concealed objects*. 2015.